Journal of Power Sources 273 (2015) 96–104

Contents lists available at ScienceDirect

Journal of Power Sources

journal homepage: www.elsevier.com/locate/jpowsour

Thermal conductivity of a graphite bipolar plate (BPP) and its thermal contact resistance with fuel cell gas diffusion layers: Effect of compression, PTFE, micro porous layer (MPL), BPP out-of-flatness and cyclic load

Hamidreza Sadeghifar [a, b], Ned Djilali [b, c], Majid Bahrami [a, *]

[a] Laboratory for Alternative Energy Conversion (LAEC), School of Mechatronic Systems Engineering, Simon Fraser University, Surrey V3T 0A3, BC, Canada
[b] Institute for Integrated Energy Systems, University of Victoria, Victoria V8W 3P6, BC, Canada
[c] Department of Mechanical Engineering, University of Victoria, Victoria V8W 3P6, BC, Canada

HIGHLIGHTS

- Thermal conductivity of graphite bipolar plates (BPP) decreases with temperature.
- Thermal Contact resistance (TCR) between BPP and GDLs decreases with compression.
- GDL-BPP TCR increases with MPL and PTFE, regardless of the PTFE loading.
- High PTFE loading, MPL, and BPP out-of-flatness increase the TCR dramatically.
- The graphite BPP-GDL TCR is a dominant resistance in a BPP-GDL assembly.

GRAPHICAL ABSTRACT

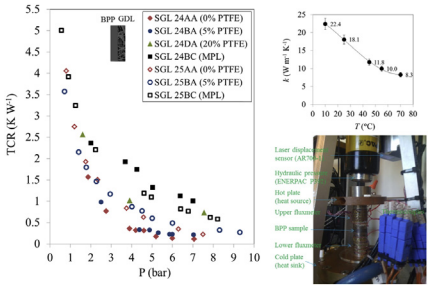

ARTICLE INFO

Article history:
Received 18 November 2013
Received in revised form
5 September 2014
Accepted 8 September 2014
Available online 18 September 2014

Keywords:
Graphite bipolar plate
Thermal conductivity
Thermal contact resistance
Gas diffusion layer
PTFE
MPL

ABSTRACT

This paper reports on measurements of thermal conductivity of a graphite bipolar plate (BPP) as a function of temperature and its thermal contact resistance (TCR) with treated and untreated gas diffusion layers (GDLs). The thermal conductivity of the BPP decreases with temperature and its thermal contact resistance with GDLs, which has been overlooked in the literature, is found to be dominant over a relatively wide range of compression. The effects of PTFE loading, micro porous layer (MPL), compression, and BPP out-of-flatness are also investigated experimentally. It is found that high PTFE loadings, MPL and even small BPP out-of-flatness increase the BPP-GDL thermal contact resistance dramatically. The paper also presents the effect of cyclic load on the total resistance of a GDL-BPP assembly, which sheds light on the behavior of these materials under operating conditions in polymer electrolyte membrane fuel cells.

* Corresponding author. Tel.: +1 (778) 782 8538; fax: +1 (778) 782 7514.
E-mail addresses: sadeghif@sfu.ca (H. Sadeghifar), ndjilali@uvic.ca (N. Djilali), mbahrami@sfu.ca (M. Bahrami).

http://dx.doi.org/10.1016/j.jpowsour.2014.09.062
0378-7753/

1. Introduction

The required power output of proton exchange membrane fuel cells (PEMFCs) for specific applications is achieved by stacking individual cells or membrane electrode assemblies (MEAs), each separated by a bipolar plate (BPP). Fig. 1 illustrates the components of a PEMFC, including the BPPs and their adjacent GDLs, and all the main thermal resistances within the cell.

The adequate thermal and associated water management of fuel cells requires knowledge of the thermal bulk and contact resistances of all involved components [1,2]. However, due to experimental difficulties, no measurements have been reported to date on the thermal contact resistance (TCR) between GDLs and graphite BPP [3–6]. Consequently, this contact resistance has either been neglected or roughly estimated in modeling studies [7–10]. The brittle, porous anisotropic nature of most fuel cell components together with their small thicknesses have made it challenging to measure their thermal resistances, e.g. see Refs. [6,11–16].

The only attempt to estimate the thermal contact resistance between BPP and GDLs to date is due to Nitta et al. [17], which was based on simulations using Fluent, with an unverified assumption of 128 W m^{-1} K^{-1} for the thermal conductivity of the graphite BPP. The reported thermal conductivity of the GDL was several times higher than typical values found in the literature and was also independent of compression. These results are inconsistent with physical observations [18–25] and with several experimental studies showing significant dependency of GDL thermal conductivity on compression [11–15,19–21].

The main purpose of the present study is to measure and analyze the behavior of thermal conductivity of the graphite BPP in terms of temperature and its thermal contact resistance with different untreated and treated GDLs over a range of compression. This work provides some key data and insights on the effect of Polytetrafluoroethylene (PTFE), micro porous layer (MPL), BPP out-of-flatness and cyclic loading on the GDL-BPP TCR.

2. Experimental setup

To measure the thermal conductivity of the graphite bipolar plates and their contact resistance with different GDLs, the thermal contact resistance (TCR) apparatus described in Ref. [6] was employed. The design of this apparatus, also called TCR machine, is based on the guarded heat flux meter device as recommended by the ASTM Standard C-177 [26]. The testbed of the TCR machine, shown in Fig. 2, is comprised of two cylindrical Armco-iron heat fluxmeters, in between which the sample is located. A temperature gradient is induced across the sample using a heat source (the hot plate) and a heat sink (the cold plate). The temperatures are measured using 12 T-type thermocouples placed inside the two fluxmeters. The heat transfer is limited to one-dimensional conduction by creating a high vacuum condition inside the test chamber. The control of the compression pressure applied on the sample is performed using a hydraulic pressure device (ENERPAC P392). The measurement and monitoring of the changes in the thickness of the compressed sample is carried out with a laser displacement sensor (AR700-1). Knowing the thermal conductivity of the fluxmeters and the measured temperature profile along them, the heat transferred through the sample and the temperature drop across it can be obtained, which yields the total thermal resistance. More details of the apparatus, the experimental testbed, and the methodology used in measuring the thermal resistances with this machine can be found elsewhere [6]. The focus here will be on the experimental procedure utilized in conducting the tests to de-convolute the contact resistance between GDLs and BPP from the other present resistances, especially for the case of GDLs containing MPL.

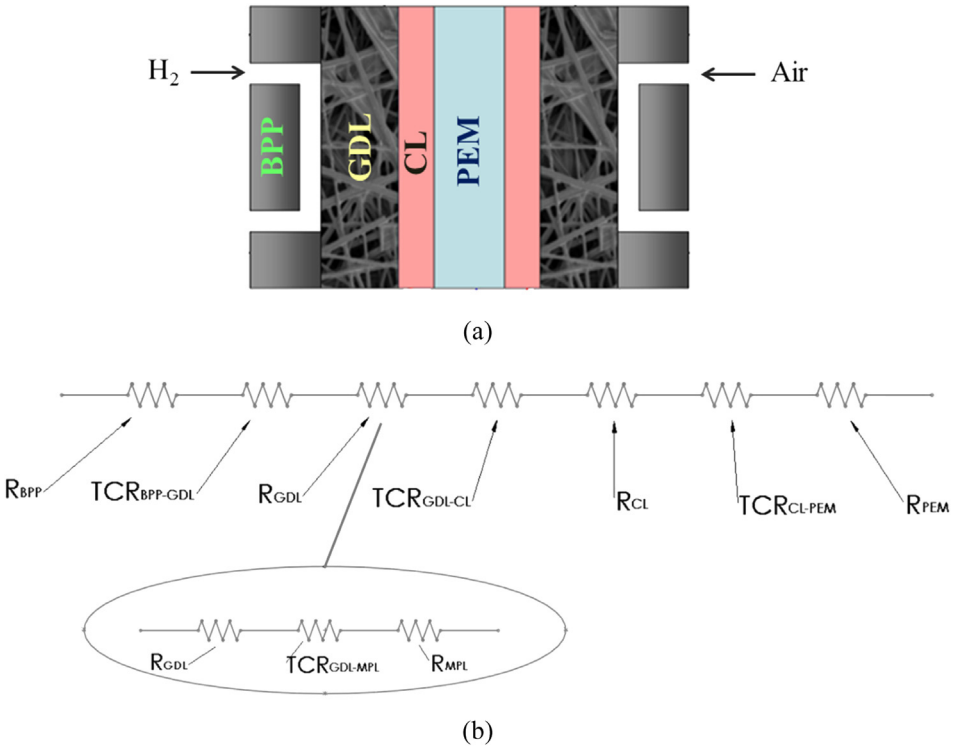

Fig. 1. (a) Main components of a PEMFC and (b) all the main thermal resistances inside a cell.

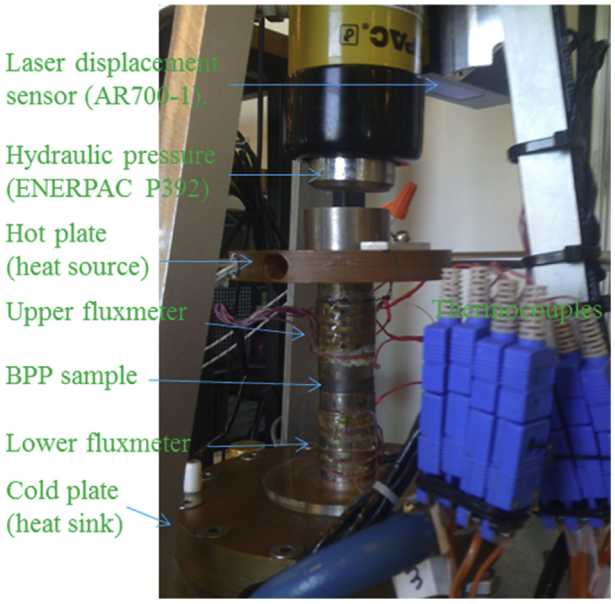

Fig. 2. Testbed of the TCR machine used for thermal resistance measurement in this study.

3. Experimental procedure and methodology

To determine the contact resistance between a BPP and a GDL, their thermal conductivities need to be known. For the accurate measurement of thermal conductivity, the two-thickness method [6] is usually employed by testing two samples of the same material with different thicknesses (see Appendix A). Hence, several tests should be first performed on each GDL and the BPP separately. To reach the BPP-GDL TCR, the total thermal resistance of a GDL-BPP assembly should be obtained. As a result, the BPP, the GDL and an assembly of the two will be tested, as schematically shown in Fig. 3. Each test is repeated at least three times to ensure that the results are repeatable and reproducible. The uncertainty in the total resistance and thermal conductivity measurements is calculated in the same manner as Refs. [4,6,7,11,13,15].

3.1. Thermal resistance (conductivity) of the graphite BPP (R_{BPP})

Applying the two-thickness method to the BPP samples with different thicknesses yields the thermal conductivity of the BPP and its contact resistance with the fluxmeters (see Appendix A). In this study, the thermal conductivity or resistance of the BPP (R_{BBP}) is required for determining its TCR with the GDLs. The tests are performed at five different temperatures to attain the thermal conductivity of the BPP as a function of temperature.

3.2. Thermal resistance (conductivity) of GDLs (R_{GDL}) and their contact resistance with the fluxmeters ($TCR_{GDL\text{-}FM}$)

Sigracet (SGL) GDLs are available in two thicknesses [6,27], which allow determining their thermal conductivity (bulk resistance: R_{GDL}) and their contact resistances with the fluxmeters (TCR_{GDL-FM}) using the two-thickness method (see Appendix A and Ref. [6] for details). The GDL bulk and contact resistances (R_{GDL} and TCR_{GDL-FM}) are both required for determining its TCR with the graphite BPP.

3.3. Thermal contact resistance between BPP and GDL ($TCR_{GDL-BBP}$)

To measure the thermal contact resistance between BPP and GDL, two GDLs with one BPP in between are sandwiched between the two fluxmeters of the TCR machine, as illustrated in Fig. 3.

The thermal resistance equation for this set of the GDL and BPP assembly is as follows:

$$2TCR_{GDL-BBP} = R_{tot} - (R_{BPP} + 2R_{GDL} + 2TCR_{GDL-FM}) \quad (1)$$

where R_{BPP}, the BPP thermal resistance, is measured in this study; R_{GDL} and TCR_{GDL-FM}, the thermal resistance (conductivity) of GDLs and their thermal contact resistances with the two fluxmeters, have originally been measured in Ref. [6]. Hence, measuring the total resistance (R_{tot}) of the components shown in Fig. 3, using the TCR machine, the contact resistance between the BPP and each GDL, $TCR_{GDL-BBP}$, can be determined using Eq. (1).

3.4. Thermal contact resistance between BPP and MPL

Micro porous layer (MPL) has become an essential component of a fuel cell stack [28,29]. It has been recently asserted [29–31] that MPL on the BPP side of GDLs can also improve the overall performance of fuel cells. Therefore, measuring the contact resistance between the MPL and BPP can be useful for the purpose of PEMFC heat management.

Gas diffusion layers with MPL on one side, such as BC type of SGL GDLs, have two different surfaces; the MPL and the substrate. The substrate is a BA-type SGL GDL, which has a carbon-based structure, called plain substrate, treated with 5% PTFE. In fact, SGL GDLs of BC type are fabricated by coating one MPL on the BA types. In order to measure the thermal contact resistance

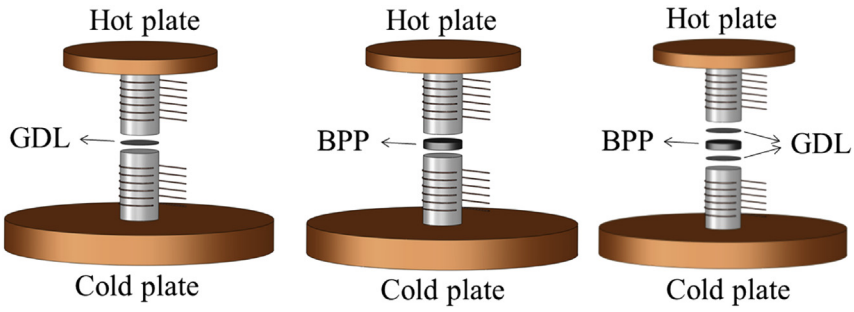

Fig. 3. Three types of experiments to be performed by the TCR machine for measuring the GDL-BPP TCR (the cylindrical fluxmeters and the thermocouples placed inside them were not labeled).

between MPL and BPP, the two GDLs are placed on both sides of the BPP, all sandwiched between the two fluxmeter, so that the MPLs always face up into the upper fluxmeter (the one contacting the hot plate). The resistance equation for such arrangement will thus be:

$$TCR_{MPL-BPP} = R_{tot_{SGL\_BC-BPP}} - (R_{BPP} + 2R_{SGL\_BC} + TCR_{MPL-FM} + TCR_{Sub5\%PTFE-FM} + TCR_{Sub5\%PTFE-BBP}) \quad (2)$$

where $TCR_{Sub5\%PTFE-FM}$ and $TCR_{Sub5\%PTFE-BBP}$ are the thermal contact resistance of the substrate BA with the (lower) fluxmeter and BPP, respectively. The values of R_{BPP}, R_{SGL_BC}, and "TCR_{MPL-FM}+$TCR_{Sub5\%PTFE-FM}$" have already been measured. Hence, there are only two unknowns, $TCR_{MPL-BPP}$ and $TCR_{Sub5\%PTFE-BBP}$, in Eq. (2). The unknown $TCR_{Sub5\%PTFE-BBP}$ can be obtained from the data of similar tests on sample SGL BA, using the following equation:

$$2TCR_{Sub5\%PTFE-BBP} = R_{tot_{SGL\_BA-BPP}} - (R_{BPP} + 2R_{SGL_{BA}} + 2TCR_{Sub5\%PTFE-FM}) \quad (3)$$

where the thermal resistance of SGL BA (substrate with 5wt% PTFE), i.e., R_{SGL_BA}, and its contact resistances with fluxmeters, $2TCR_{Sub5\%PTFE-FM}$, have already been measured and reported in Ref. [6]. Plugging the value of $TCR_{Sub5\%PTFE-BBP}$, obtained from Eq. (3), into Eq. (2) yields the target parameter of the thermal contact resistance between MPL and BPP, i.e., $TCR_{MPL-BBP}$.

3.5. BPP samples

Three graphite bipolar plate blank samples of the same material (machined from one plate) with different thicknesses of 2.95, 4.94, and 5.84 mm, herein referred to in terms of their thicknesses, were employed for thermal conductivity measurements. Before performing any measurements, some surface analysis tests were carried out on all three samples to ensure the acceptable flatness of the sample surfaces. The deviations in the flatness of the sample surfaces, obtained by a surface dial indicator (Mitutoyo) (Fig. 4), are summarized in Table 1.

In order to measure the most accurate thermal conductivity values using the two thickness method, samples 2.95 and 5.84 showing proper surface flatness are selected. Sample 4.94 is only used later for investigating the effect of BPP out-of-flatness on its thermal contact resistance with GDLs.

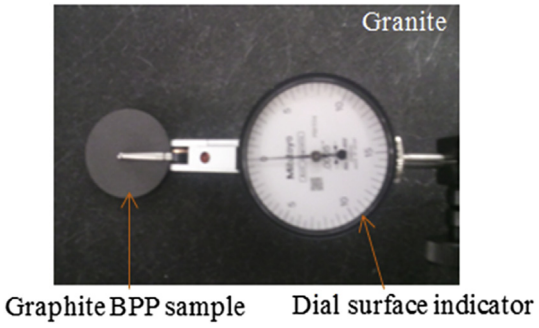

Fig. 4. Measuring deviations in the flatness of the BPP sample surfaces with a dial test indicator.

Table 1
Maximum deviations in the flatness of the studied samples' surfaces.

Sample thickness (mm)	2.95	4.94	5.84
	Maximum deviation in flatness (mm)/0.0127		
One surface	0.5	<1.5	0.5
The other surface	<0.5	<0.75	<0.5

4. Results and discussion

4.1. Thermal conductivity of the graphite BPP

The thermal conductivity of the graphite BPP is plotted as a function of temperature and compression in Fig. 5. The thermal conductivity does not change with compression, as expected; however, it increases with decreasing temperature. The temperature dependency of the BPP thermal conductivity, shown in Fig. 6, can be approximated by a third-order polynomial equation as:

$$k = \left(5.713 \times 10^{-5}\right)T^3 - \left(4.653 \times 10^{-3}\right)T^2 - 0.188T + 24.718 \quad (4)$$

where k and T represent thermal conductivity (W m^{-1} K^{-1}) and temperature (°C), respectively. The slope of the k–T curve decreases with increasing temperature from 10 to 70 °C.

The TCR between the BPP and the Armco-iron fluxmeters decreases with both pressure and temperature, as shown in Fig. 7. The results show that the effect of temperature on this TCR is, however, much stronger than that of compression. The descending trend of the TCR with temperature is similar to the trends observed for the data of other solid–solid contact resistance available in the literature; see e.g. Ref. [32].

4.2. Thermal conductivity of GDLs and their contact resistance with the fluxmeters

A thorough study on the thermal conductivity of different treated and untreated SGL GDLs, series 24 & 34, as well as series 25

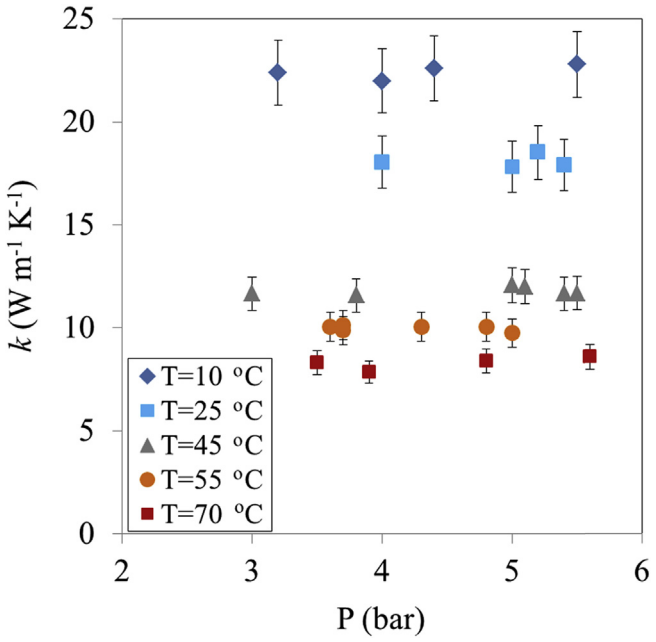

Fig. 5. Thermal conductivity of the graphite BPP (k_{BPP}) at different temperatures and compression (obtained from repeated tests): $R_{BBP} = t_{BBP}/k_{BPP}A$.

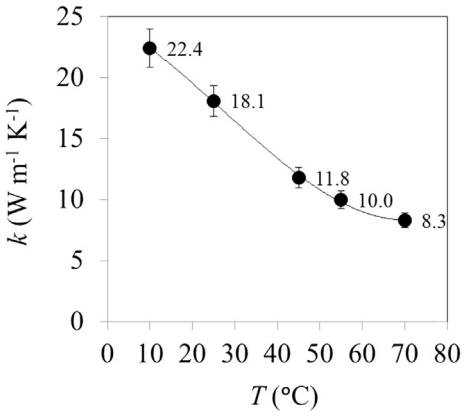

Fig. 6. Thermal conductivity of the graphite BPP (k_{BPP}) as a function of temperature.

and 35, and their TCR with the same Armco-iron fluxmeters have been performed in the authors' pervious work [6]. Here the thermal conductivity of all studied GDLs is presented, as a function of compression, in one graph (Fig. 8) and the GDL-fluxmeter TCRs are also included (Fig. 9) to facilitate the data analysis and comparison. The variation of the GDL thickness with compression, already reported in Ref. [6], is considered in all the calculations, see Eqs. (A1–3) of Appendix A.

4.3. Thermal contact resistance between GDL and BPP ($TCR_{GDL\text{-}BPP}$)

Knowing the thermal conductivity of the BPP and those of GDLs and the thermal contact resistance between GDLs and fluxmeters, the thermal contact resistance between the BPP and GDLs can be determined as explained in Section 3. The BPP-GDL TCRs presented in Fig. 10 for different SGL show that the TCR for all the GDLs decreases with compression. The interesting point to note here is that the reduction rate of $TCR_{GDL\text{-}BPP}$ with compression load decreases with increasing pressure, regardless of the GDL type. In fact, at

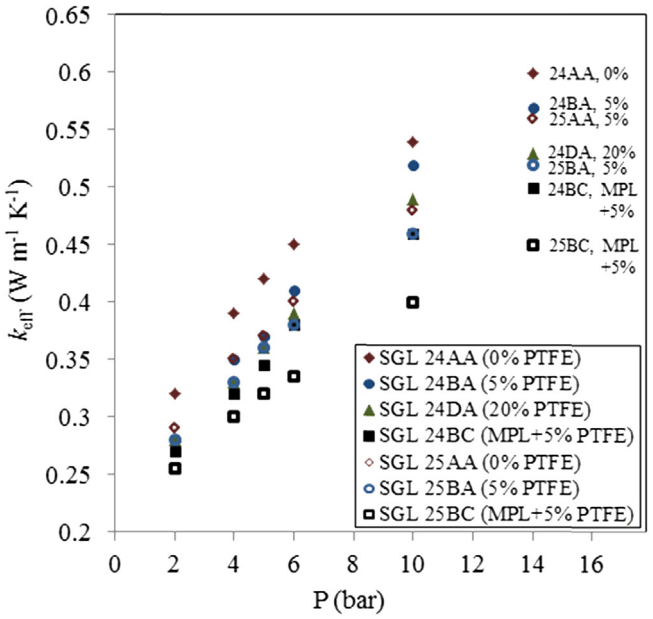

Fig. 8. Thermal conductivity of Sigracet untreated and treated GDLs (k_{GDL}) as a function of compression: $R_{GDL} = t_{GDL}/k_{GDL}A$.

lower compression, the $TCR_{GDL\text{-}BPP}$ is much more sensitive to compression for all the GDLs, and as the pressure increases, the dependency of $TCR_{GDL\text{-}BPP}$ on the pressure decreases.

- Effect of PTFE loading and MPL

Fig. 10 also indicates that for both series of the studied SGLs, i.e., 24 & 34 and 25 & 35, PTFE practically increases the $TCR_{GDL\text{-}BPP}$, which is similarly to the increasing effect of PTFE on the TCR between GDLs and the fluxmeters, as discussed in Ref. [6]. From Fig. 10, it is also observed that the effect of 5% PTFE on the $TCR_{GDL\text{-}}$

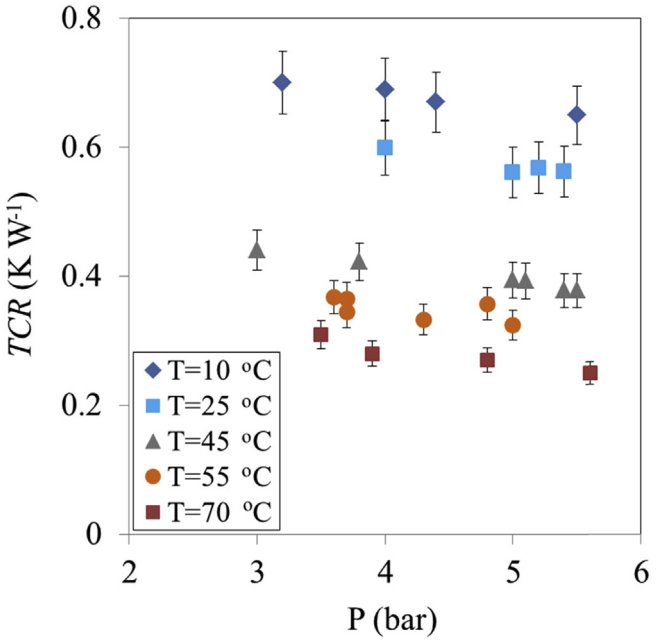

Fig. 7. TCR between the graphite BPP and the Armco-iron fluxmeters at different temperatures and compression (obtained from repeated tests).

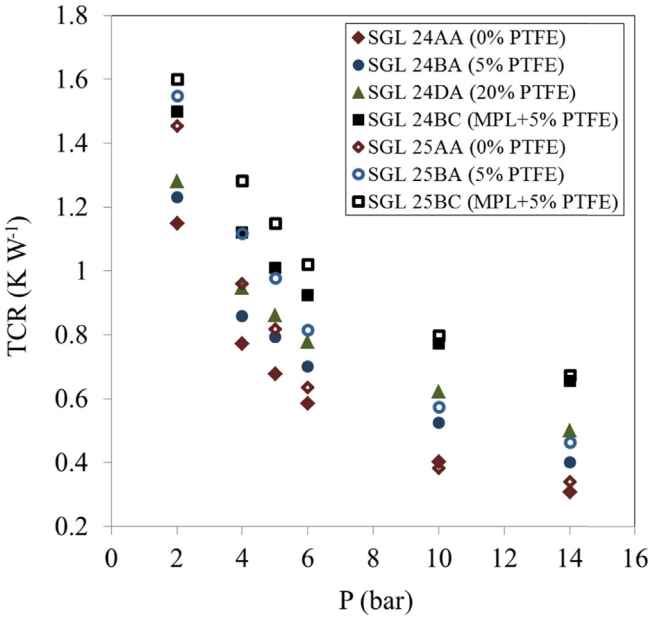

Fig. 9. Thermal contact resistances of Sigracet untreated and treated GDLs with the Armco-iron fluxmeters (FM) as a function of compression: TCR_{GDL-FM} & TCR_{MPL-FM}.

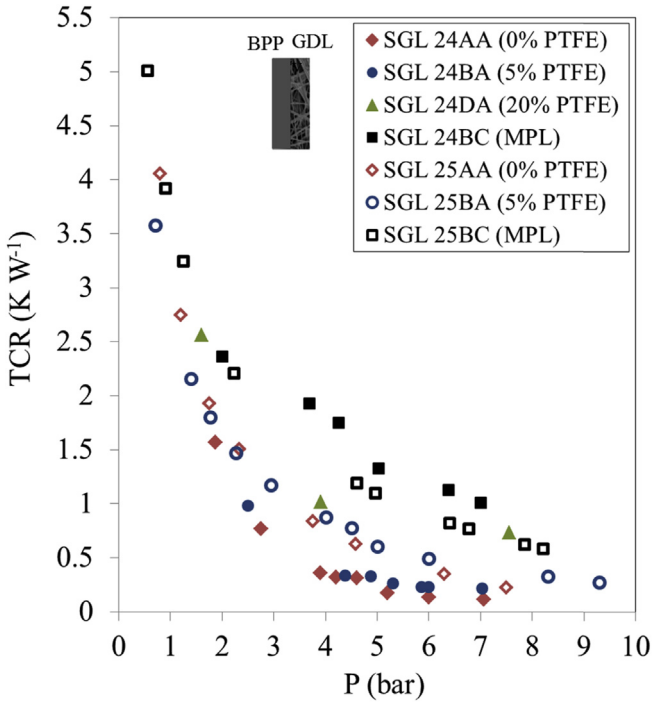

Fig. 10. Experimental data of TCR between the graphite BPP and 14 different SGL GDLs ($TCR_{GDL\text{-}BPP}$) at an average temperature of 55 °C.

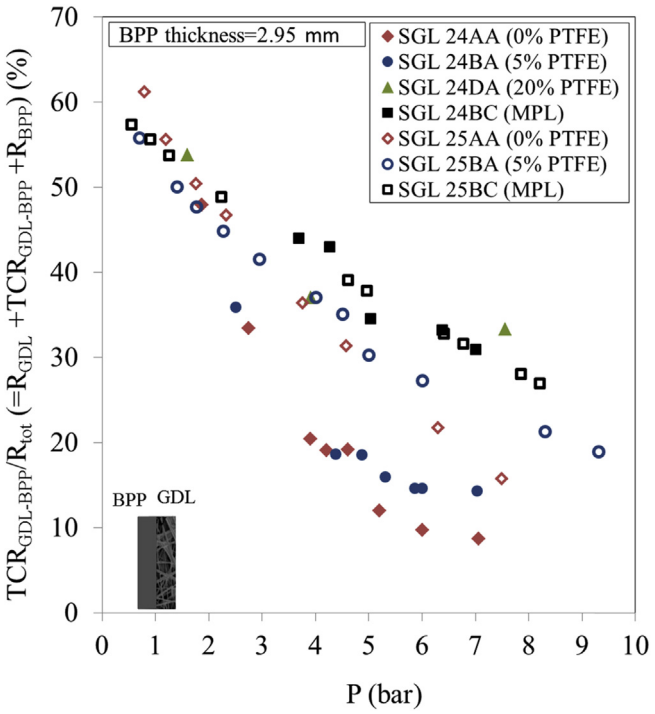

Fig. 11. Contribution of the TCR between the graphite BPP and different SGL GDLs into the total resistance of the studied BPP-GDL assemblies at an average temperature of 55 °C.

$_{BPP}$ is minimal, whereas the addition of 20 wt% PTFE to the plain substrate increases the $TCR_{GDL\text{-}BPP}$ dramatically, especially at the higher pressures. For series 24 & 34 of SGLs, the effect of 20 wt% PTFE on the $TCR_{GDL\text{-}BPP}$ is comparable to that of MPL, which has the highest impact on the $TCR_{GDL\text{-}BPP}$ in comparison to the other GDLs of series 24.

It is also interesting to note that the effect of MPL on the BPP-GDL TCR is the same for both series. The MPL markedly increases the TCR, especially in comparison to GDLs treated with low PTFE loadings. In addition, the BBP-MPL TCR for both series of the studied GDLs are very close to each other because the MPLs employed for both series are practically the same [6,27].

It is also observed that at low compression, there is no appreciable difference between the TCRs of BPP with different GDLs. In other words, the dependency of the TCR on PTFE loadings and MPL increases with compressive load for most of the GDLs.

The contribution of $TCR_{BPP\text{-}GDL}$ to the GDL-BPP total resistance has been shown on Fig. 11 for different GDLs, to further investigate the importance of $TCR_{BPP\text{-}GDL}$ with regard to the bulk resistances of GDL and BPP. Fig. 11 shows that the $TCR_{BPP\text{-}GDL}$, a parameter that has been usually overlooked in fuel cell thermal analysis, is indeed a large resistance comparable to the GDL and BPP resistances, especially for the GDLs treated with high PTFE loadings and MPL. For instance, the TCR between BPP and SGL 24DA is approximately 40% of the total resistance at the compression of 4 bar, which makes it the dominant resistance, as the bulk resistance of GDL and BBP contribute, respectively, 35 and 25% to the total resistance.

Fig. 11 also indicates that $TCR_{BPP\text{-}GDL}$ for SGL 25 is, to some extent, larger than that for SGL 24. The reason for this is most likely related to the higher porosity and the lower aspect ratio SGL 25 has, as these are the only difference between the two series 24 and 25, see Ref. [12].

It is also worthwhile noting that the contribution of $TCR_{BPP\text{-}GDL}$, which increases dramatically with decreasing the load, reaches approximately 60% and 40% of the total resistance for most of GDLs at the compression of 1 and 5 bar, respectively. The fact that $TCR_{BPP\text{-}GDL}$ is usually the dominant resistance in GDL-BPP thermal resistance network is an important finding that underscores the need to fully account rather than neglect thermal resistance compared to the bulk resistance of BPP and GDL in fuel cell thermal management and modeling.

4.4. Effect of BPP out-of-flatness on TCR

The remarkable impact of BPP out-of-flatness on the $TCR_{BPP\text{-}GDL}$ can be observed in Fig. 12 where a comparison between the TCR of different SGLs 24 with two BPP plates with different out-of-flatness can be made. Fig. 12 shows that the TCR of the GDLs with bumpy BPP 4.94 is much higher than that with more flat BPP 5.84. It should be noted that based on Table 1, BPP 4.94 is not excessively wavy and its out-of-flatness would be considered low from the viewpoint of contact mechanics [33,34]. Nevertheless, even such low out-of-flatness can lead to large $TCR_{BPP\text{-}GDL}$, according to Fig. 12. Overall, the out-of-flatness of BPP 4.94 increased the $TCR_{BPP\text{-}GDL}$ by a factor of 3, on average.

The results in Fig. 12 indicate that the BPP out-of-flatness can exacerbate the influence of PTFE and MPL on the TCR, as the gap between the TCR of the untreated SGL 24 (24AA) and the treated ones with BPP 4.94 are larger than the corresponding values for more flat BPP 5.84.

4.5. Effect of cyclic load on total resistance

The effect of cyclic load on the total resistance of two SGL 24BA, as well as separately on two SGL 24DA, with BPP 5.84 in between, all sandwiched between the two fluxmeters of the TCR machine, are presented in Figs. 13 and 14, respectively. As seen in both Figs. 13 and 14, overall, the load cycles, especially the initial ones, reduce

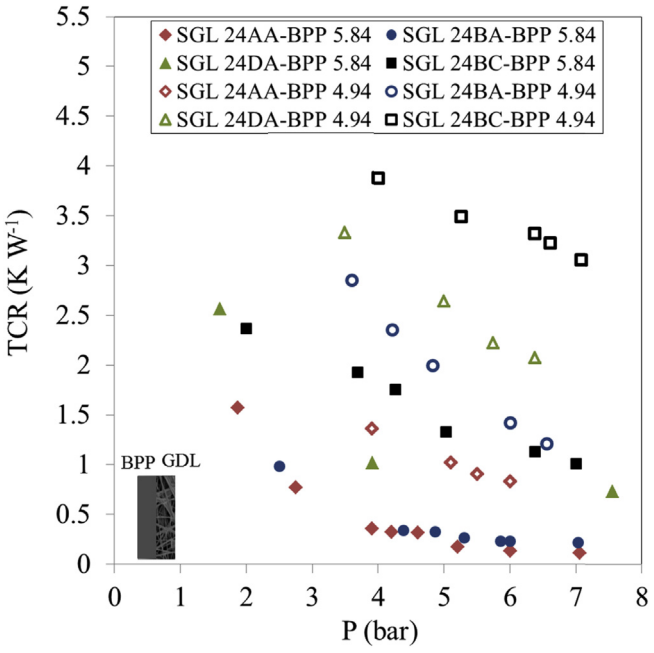

Fig. 12. Effect of the BPP out-of-flatness on $TCR_{BPP\text{-}GDL}$ (for comparison, the data of SGL 24 already shown in Fig. 11 has been duplicated in this figure).

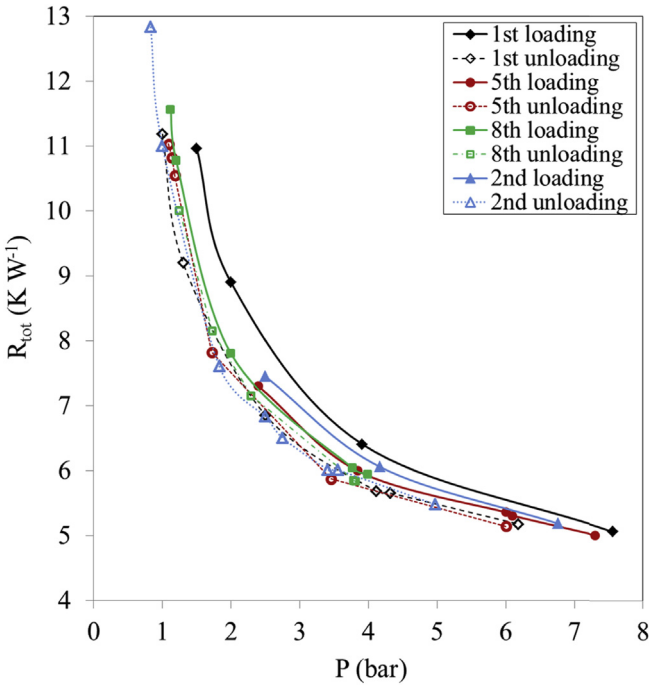

Fig. 14. Effect of load cycles on the total resistance of SGL 24DA-BPP 5.84 assembly (including the contact resistance of the GDL with the two fluxmeters).

the total resistance. This reduction is more pronounced for SGL 24BA, due to having lower PTFE loading (5%) in comparison to SGL 24DA, which has treated with 20% PTFE.

It is also evident from Figs. 13 and 14 that at high compression, the data of different loadings tend to overlap, which completely conforms with the trend obtained for the cases of one GDL sandwiched between the same two fluxmeters of the TCR machine [6,12]. No noticeable difference between the 3rd loading and unloading has been observed for SGL 24BA whereas the gap between the successive loadings and unloadings for SGL 24DA is considerable, especially for the initial cycles, as evident in Fig. 14. Overall, knowledge of the thermal resistance behavior of GDL-BPP assembly under different load cycles, as reported here, can inform the analysis of the temperature field within operating PEMFCs and the design of appropriate heat and water management during their lifetime.

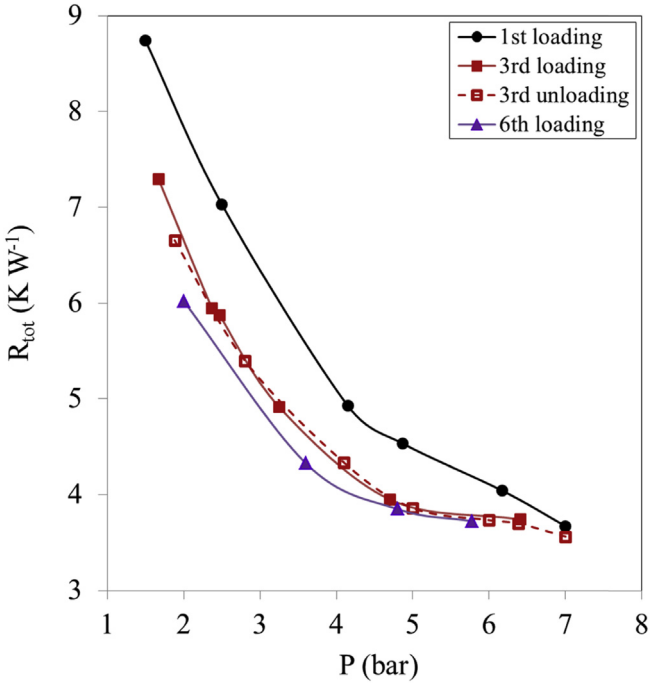

Fig. 13. Effect of load cycles on the total resistance of SGL 24BA-BPP 5.84 assembly (including the contact resistance of the GDL with the two fluxmeters).

5. Summary and conclusion

Thermal conductivity of a graphite BPP was measured under different temperatures and pressures, with the following key results:

- Thermal conductivity of the graphite BPP and its thermal contact resistance with the Armco-iron fluxmeters decrease with increasing temperature.
- The variation of the BPP thermal conductivity in terms of temperature can be conveniently represented in a compact form suitable for thermal analysis and modeling

The TCR between the BPP and GDLs with different PTFE loadings and/or MPL were also measured in terms of compression. The effect of compression, PTFE, MPL, out-of-flatness, and cyclic loads on the BPP-GDL TCR were investigated thoroughly:

- The TCR between BPP and GDL increases with both MPL and PTFE, regardless of the PTFE loading.
- High PTFE loading, MPL, and the BPP out-of-flatness increase the GDL-BPP TCR dramatically.
- The BPP-GDL TCR can be the dominant resistance in GDL-BPP assembly, as its contribution can increase to almost 60% and 40% at the compression of 1 and 5 bar, respectively.

- Load cycling reduces the total thermal resistance of BPP-GDL assembly considerably.
- The reduction effect of load cycling on the thermal resistance of BPP-GDL assembly is more pronounced for GDLs with lower PTFE loading.

Acknowledgment

Ballard Power Systems is gratefully appreciated for its collaboration on this research project, especially for providing some of the samples. The first author also appreciates SGL Carbon Company for providing the GDL samples and also for some technical guidance regarding the SGL GDLs specifications.

Appendix A

Using two samples of the same material with different thicknesses t_1 and t_2, the bulk resistance (thermal conductivity) can be deconvoluted from the contact resistance of the sample. The total value of the thermal resistance for each sample can be written as (Fig. A1):

$$R_{tot_1} = \frac{t_1}{kA} + 2TCR \tag{A1a}$$

$$R_{tot_2} = \frac{t_2}{kA} + 2TCR \tag{A1b}$$

where k represent the thermal conductivity of the sample and A is the cross-sectional area of the fluxmeters and of the sample. TCR represents the thermal contact resistance between the sample and the fluxmeters, which is, unlike the bulk resistance $t_i/kA = R_i$ ($i = 1, 2$), independent of the sample thickness (Fig. A2). R_{tot}, the total resistance, is the only measurable resistance here.

The sample thermal conductivity k and the TCR are the two unknowns that can be obtained from two Eq. (A1a) and (A1b):

$$k = \frac{(t_2 - t_1)}{(R_{tot_2} - R_{tot_1})A} \tag{A2}$$

$$TCR = \frac{(t_2 R_{tot_1} - t_1 R_{tot_2})}{2(t_2 - t_1)} \tag{A3}$$

This accurate and effective way of de-convoluting thermal contact resistance (TCR) from bulk, and in fact from measurable total resistance, is called two-thickness method.

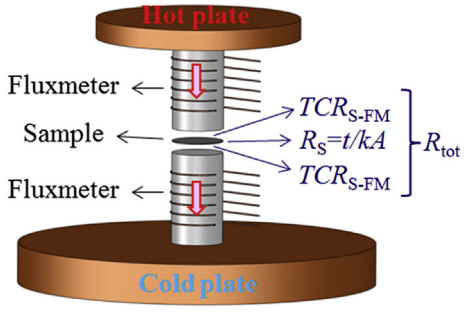

Fig. A1. The measurable thermal resistance (R_{tot}) of a sample (S) with thermal conductivity k, thickness t and cross-sectional area A, and its resistance components, including the two TCRs between the sample (S) and the two fluxmeters (FMs): The heat (shown as the red arrows) is transferred from the hot plate to the cold plate through the sample and the fluxmeters, all embedded inside a vacuum chamber.

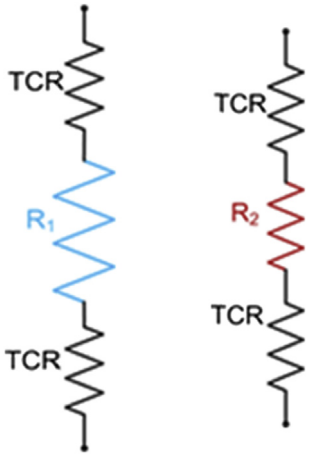

Fig. A2. Thermal resistance network for samples with different thicknesses ($R_1 = t_1/kA$ and $R_2 = t_2/kA$) (see Fig. A1).

References

[1] EG&G Technical Services, Fuel Cell Handbook, Parsons, Inc., Morgantown, West Virginiak, 2000.
[2] N. Djilali, Energy 32 (2007) 269–280.
[3] M.M. Mench, Fuel Cell Engines, John Wiley & Sons, 2008.
[4] H. Sadeghifar, M. Bahrami, N. Djilali, Thermal conductivity of graphite bipolar plate and its thermal contact resistance with gas diffusion layers: Part II. Effect of PTFE, MPL, compression, cyclic load and hysteresis behavior, in: Hydrogen & Fuel Cell Conference, June 16–19, Vancouver, BC, Canada, 2013.
[5] M.K. Debe, Nature, http://dx.doi.org/10.1038/nature11115.
[6] H. Sadeghifar, M. Bahrami, N. Djilali, J. Power Sources 248 (2014) 632–641.
[7] H. Sadeghifar, M. Bahrami, N. Djilali, in: ASME 11th Fuel Cell Science, Engineering and Technology Conference, July 14–19, Minneapolis, MN, USA, 2013. Paper No. ES-FuelCell2013-18070.
[8] P. Zhou, C.W. Wu, J. Power Sources 170 (2007) 93.
[9] T. Hottinen, O. Himanen, S. Karvonen, I. Nitta, J. Power Sources 171 (2007) 113.
[10] H. Sadeghifar, N. Djilali, M. Bahrami, in: 11th International Conference of Numerical Analysis and Applied Mathematics, September 21–27, Rhodes, Greece, 2013.
[11] H. Sadeghifar, M. Bahrami, N. Djilali, Thermal conductivity of Sigracet gas diffusion layers and MPL: Part I, in: Effect of Compression, PTFE, MPL, Cyclic Load and Hysteresis Behavior, Hydrogen & Fuel Cell Conference, June 16–19, Vancouver, BC, Canada, 2013.
[12] H. Sadeghifar, M. Bahrami, N. Djilali, J. Power Sources 233 (2013) 369–379.
[13] E. Sadeghi, N. Djilali, M. Bahrami, J. Power Sources 196 (2011) 246–254.
[14] E. Sadeghi, N. Djilali, M. Bahrami, J. Power Sources 195 (2010) 8104–8109.
[15] E. Sadeghi, N. Djilali, M. Bahrami, J. Power Sources 196 (2011) 3565–3571.
[16] M.F. Mathias, J. Roth, J. Fleming, W. Lehnert, Diffusion media materials and characterisation, in: W. Vielstich, H.A. Gasteiger, A. Lamm (Eds.), Handbook of Fuel Cells: Fundamentals, Technology and Applications, John Wiley, New York, 2003.
[17] I. Nitta, O. Himanen, M. Mikkola, Fuel Cells 08 (2) (2008) 111–119.
[18] D.L. Wood, R.L. Borup, Durability aspects of gas-diffusion and microporous layers, in: Felix N. Büchi, Minoru Inaba, Thomas J. Schmidt (Eds.), Polymer Electrolyte Fuel Cell Durability, Springer, New York, 2009, pp. 159–195, http://dx.doi.org/10.1007/978-0-387-85536-3.
[19] H. Sadeghifar, M. Bahrami, N. Djilali, in: ASME 10th Fuel Cell Science, Engineering and Technology Conference, July 23–26, San Diego, CA, USA, 2012. Paper No. ESFuelCell2012-91160.
[20] H. Sadeghifar, N. Djilali, M. Bahrami, Role of micro porous layer (MPL) in electrical and thermal resistances of fuel cell gas diffusion layers (GDLs), in: 97th Canadian Chemistry Conference and Exhibition, Vancouver, BC, Canada, June 1–5, 2014.
[21] H. Sadeghifar, N. Djilali, M. Bahrami, J. Power Sources 266 (2014) 51–59.
[22] H. Sadeghifar, N. Djilali, M. Bahrami, Analytical modeling of thermal contact resistance between gas diffusion layers and microporous layers of polymer electrolyte membrane fuel cells, (submitted for publication), 2014.
[23] H. Sadeghifar, N. Djilali, M. Bahrami, A novel approach to measuring in-plane electrical conductivity of a catalyst coated membrane (CCM) and its electrical contact resistance with fuel cell gas diffusion layers (GDLs) and micro porous layers (MPLs): Effect of compression, PTFE and humidity, in: 97th Canadian Chemistry Conference and Exhibition, Vancouver, BC, Canada, June 1–5, 2014.
[24] H. Sadeghifar, M. Bahrami, Thermal conductivity of Ballard's Bipolar Plates, Ballard technical report, No. BPP-0926–12/1, Laboratory for Alternative Energy Conversion, Simon Fraser University, Vancouver, BC, Canada, September 2012.
[25] H. Sadeghifar, M. Bahrami, Thermal and Electrical Resistances of Mercedes Benz Fuel Cell Samples: Effects of Compression, Temperature, Load Cycling,

and Assembly, Mercedes Benz Fuel Cell (MBFC) technical report, No. MEAGDLCCM-1030–13/1, Laboratory for Alternative Energy Conversion, Simon Fraser University, Vancouver, BC, Canada, October 2013.
[26] ASTM Standard C-177, Standard Test Method for Steady-state Heat Flux Measurements and Thermal Transmission Properties by Means of the Guarded Hot-plate Apparatus, ASTM International, Conshohocken, PA, 1985.
[27] SGL Group – The Carbon Company. SIGRACET Diffusion Media, Manufacture Data Sheet. Web: http://www.sglgroup.com/cms/international/home.
[28] N. Furuya, N. Mineo, J. New. Mater. Electrochem. Syst. 10 (2007) 205–208.
[29] J.D. Sole, Investigation of Novel Gas Diffusion Media for Application in PEM Fuel Cell Ribbon Assemblies, M.S. thesis, Virginia Polytechnic Institute and State University, USA, 2005.
[30] M.M. Mench, E.C. Kumbur, T. Nejat Veziro glu (Eds.), Polymer Electrolyte Fuel Cell Degradation, Academic Press (Elsevier), MA, USA, 2012.
[31] X.L. Wang, H.M. Zhang, J.L. Zhang, H.F. Xu, Z.Q. Tian, J. Chena, H.X. Zhong, Y.M. Liang, B.L. Yi, Electrochim. Acta 51 (2006) 4909–4915.
[32] D. Bi, H. Chen, T. Ye, Cryogenics 52 (2012) 403–409.
[33] M.M. Yovanovich, W.M. Rohsenow, Influence of Surface Roughness and Waviness upon Thermal Contact Resistance, Technical Report No. 6361–48, Contract No. Nas T-100, Massachusetts Institute of Technology, USA, 1967.
[34] S. Sunil Kumar, K. Ramamurthi, ASME J. Heat Transf. 125 (2003) 394–402.

Nomenclature

AA,BA,DA,BC: different types of Sigracet GDLs (0,5,20, 5(& MPL on one side) %PTFE, respectively)
BPP: bipolar plate
GDL: gas diffusion layer
k: thermal conductivity, W m^{-1} K^{-1}
MPL: micro porous layer
P: compression, bar or kPa
PEMFC: polymer electrolyte membrane fuel cell
PTFE: polytetrafluoroethylene
R: thermal resistance, KW^{-1}
SGL: Sigracet
T: temperature, °C or K
TCR: thermal contact resistance
wt%: weight percent

Subscript

BPP: bipolar plate
FM: fluxmeter
GDL: gas diffusion layer
MPL: micro porous layer
SGL: Sigracet
SGL_BA: Sigracet GDLs of type BA
SGL_BC: Sigracet GDLs of type BC
sub: substrate of GDLs containing MPL
tot: total